Negative Refraction and Imaging in Photonic Crystals

S. Sridhar[1], P. V. Parimi, W. T. Lu, and P. Vodo,
Electronic Materials Research Institute and Physics Department, Northeastern University
360 Huntington Avenue, Boston, MA 02115.
John S. Derov,
AFRL Hanscom, Bedford, MA.

ABSTRACT

Negative refraction and left-handed electromagnetism in a photonic crystal are demonstrated in waveguide and free space experiments at microwave frequencies. Precision control to achieve tailor-made refractive indices has been achieved. The negative refraction in these photonic crystals is shown to lead to imaging by a flat lens. We have also developed a generalized theory of flat lens imaging. These results promise potential applications in a variety of optical and microwave systems for communications and imaging.

1. Introduction

Negative refraction (NR) is a new phenomenon allowed by Maxwell's equations that has led to novel effects regarding the propagation and control of electromagnetic waves. In a negatively refracting material, electromagnetic waves obey a left-handed relationship between the vectors **E**, **H** and **k**, and hence the media are also referred to as left-handed metamaterials (LHM). NR has been recently demonstrated in two types of LHM - composite metamaterials [i,ii,iii] made of split ring resonators and wire strips, and in photonic crystals (PC) [iv,v].

Negative refraction in LHM leads to new optical and electromagnetic components that open the door for new applications from microwave to optical frequencies. An interesting application of negative refraction is superlensing[vi] effect by a flat lens with no curved surfaces that can potentially overcome the diffraction limit imposed by conventional lenses. We have recently fabricated a flat lens recently using a photonic crystal structure and demonstrated focussing without optical axis[vii]. The flat lens is best suited when the source is close to the surface of the lens. For those applications where imaging of far objects is important, we have recently demonstrated focusing by a plano-concave lens using negative refraction, thus enabling several applications of far field imaging[viii].

In this paper we describe the experimental setups and results that demonstrate negative refraction in photonic crystals. The experimental results are in excellent agreement with band structure calculations. A generalized theory of imaging by a flat lens is briefly described, accompanied by numerical confirmation of imaging by a lens composed of periodic scatterers. These results confirm the experimental results reported earlier in real photonic crystal flat lens experiments.

2. Experimental setups

We have carried out two types of experiments that demonstrate negative refraction in PC, parallel plate waveguide[ix,x] and free space experiments inside an anechoic chamber[xi]. In both cases microwave refraction measurements were carried out on wedge prisms fabricated from PC structures, and negative refraction was clearly observed.

2.1. Parallel Plate Waveguide experiments

The microwave photonic crystal consists of an array of cylindrical copper rods with a radius 0.63 cm arranged in a triangular lattice. The ratio of the radius r to lattice constant a is kept at $r/a = 0.2$. Refraction measurements are

[1] s.sridhar@neu.edu

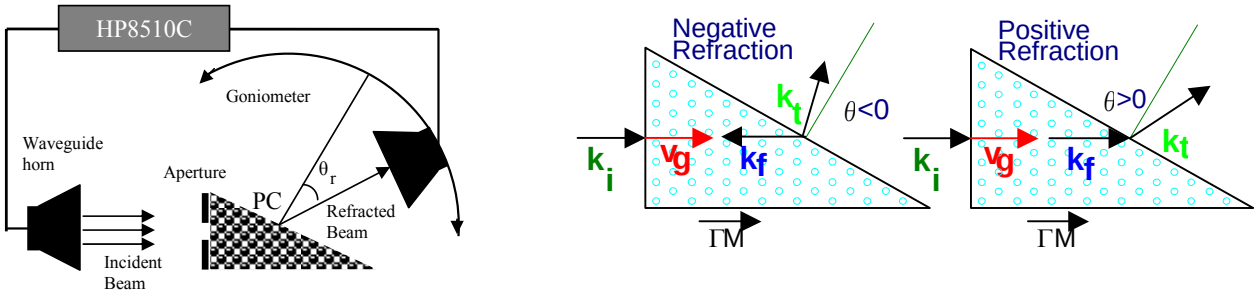

Figure 1 (Left) Free space experimental setup for microwave refraction measurements. (Right) Directions of the wavevectors and the group velocity in the refraction experiments for negative and positive refraction.

carried out in a metallic parallel plate waveguide. The excitation inside this waveguide is transverse magnetic (TM), meaning that the electric field E_y, is parallel to the axis of the dielectric rods. The collimated microwave beam propagates a distance of ~1m in the waveguide, and then is incident normally to the PC wedge (see Fig. 1).

The other face of the prism, which is the surface of refraction, is at 60^0 to the incident beam. A dipole antenna is mounted on a goniometer that runs along the semicircular outer edge of the parallel plate waveguide to detect the refracted beam. The refraction is considered positive (negative) if the emerging beam is detected at positive (negative) angles as shown in Fig 1.

The calibration of the refraction experiment set up is validated by the refraction experiment performed on a polystyrene prism of the similar dimensions to the PC prism that corresponds to a positive refractive index $n = 1.58$ as expected by theory.

2.2. Free Space Experiments

In addition to the parallel plate experiments described above, we also carried out free space (FS) experiments using metallic PC prism suspended in air. The principal advantage of these free space experiments is the ability to separate out beams over large transmission distances of 3m. Furthermore, the polarization can be varied and refraction experiments were carried out for both for both TM ($\vec{E}$ || to the rod axis) and TE ($\vec{E}$ ⊥ to the rod axis) mode propagation. Excellent agreement with band structure calculations was observed for both polarizations, showing that a PC can exhibit negative refraction with tailor made refractive indices in a large frequency range.

The microwave photonic crystal consists of an array of cylindrical copper tubes arranged on the same periodical triangular lattice as described in the above parallel plate waveguide experiment. Refraction experiments were performed in an anechoic chamber of dimensions 5 x 8 x 4 m^3 to prevent reflections from the walls. A square X-band horn placed at 3 m from the PC acts as a plane wave source (Fig.1). A piece of microwave absorber with a 6x6$inch^2$ aperture in front of the PC was used to narrow the incident beam. On the far side another square horn was attached to a goniometer which swings around in two-degree steps to receive the emerging beam. Refraction is considered positive (negative) if the emerging signal is received to the right (left) of the normal to the surface of refraction of the PC. Measurements were carried out with the incident wave vector $\vec{k}_i$ along $\Gamma \to M$ (0,1) direction of the first Brillion zone of the PC and in both TM and TE modes. The angle of incidence $\theta = 60°$ for $\Gamma \to M$ is chosen in order to minimize surface periodicity along the surface of refraction, thus eliminating higher order Bragg waves.

3. Results

A 3D plot of the transmitted intensity measured at different angles in the frequency window 6-12GHz for the TM mode propagation is shown if Fig. 2 b2. Also shown are polar plots of the transmitted intensity at selected frequencies 6.68, 9.315 and 10.77 GHz showing the emerging beams.

As can be seen from the figure between 6 and 7.1 GHz the signal emerges on the positive side of the normal to the surface corresponding to positive refraction. No transmission is observed between 7.1 and 8.3 GHz. Above 8.3 GHz and 11 GHz two signals are observed on the positive and negative sides of the normal corresponding to 1st and 0th order Bragg wave refraction. The negatively refracted signal is strongest from 10.14 -11GHz and positively refracted signal around 8.6-9.6 GHz and in the frequency window 9.6-10.14 GHz both signals have the same strength. So with the increase in frequency the positive signal gets weaker while negative signal gets stronger. The experimental refractive index n is obtained from applying Snell's law $n = \sin(\theta_r)/\sin(\theta_i)$ to each emerging beam. The validity of Snell's law has been established earlier in metallic PCs (ix).

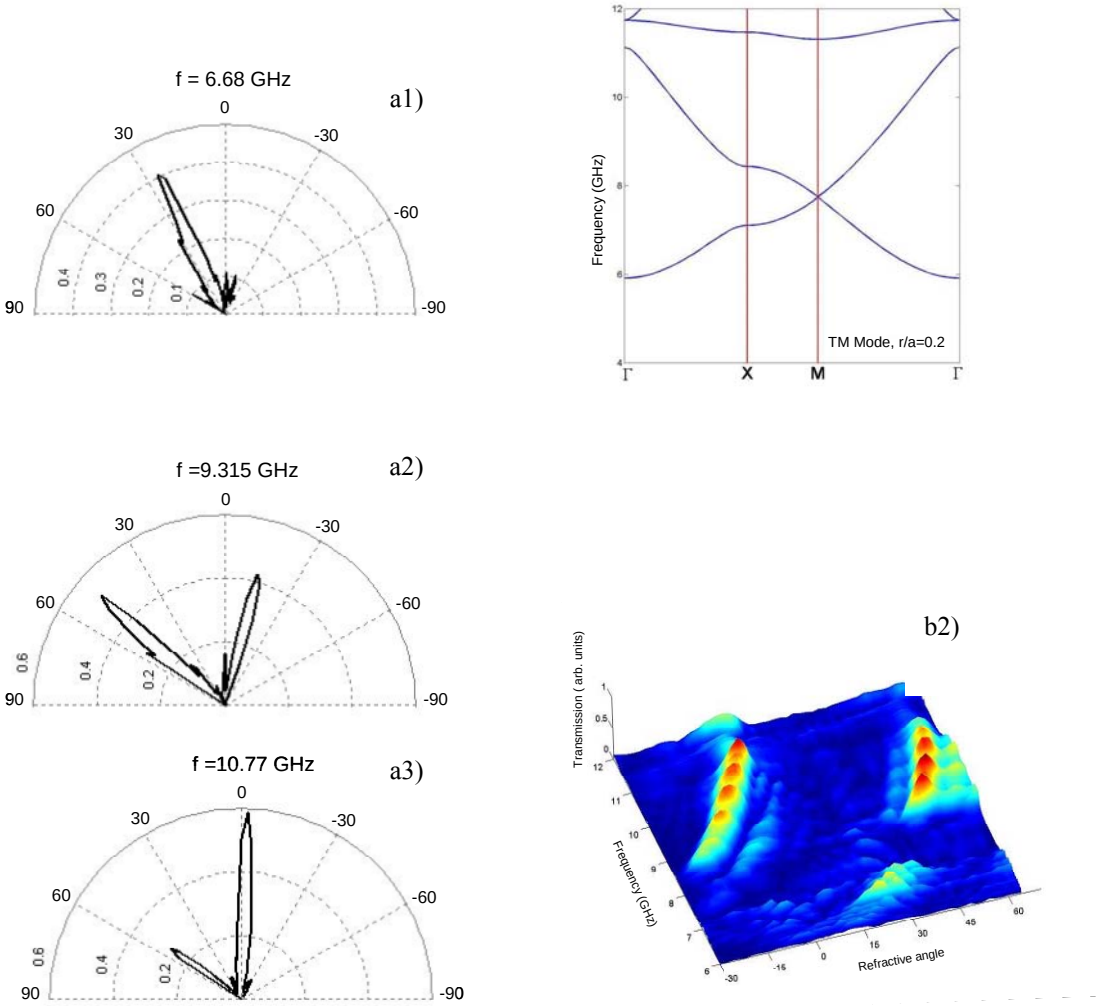

Fig. 2 Figures 2 a1, a2, a3 show polar plots of wave directivity for representative frequencies of 6.68 GHz, 9.315 GHz and 10.77GHz. Figure 3b1 shows the band structure of the triangular lattice of metallic PC with packing density r/a=0.2 for TM Mode and Figure 2b2 shows the 3D experimental map of the refracted field versus frequency and angle of refraction.

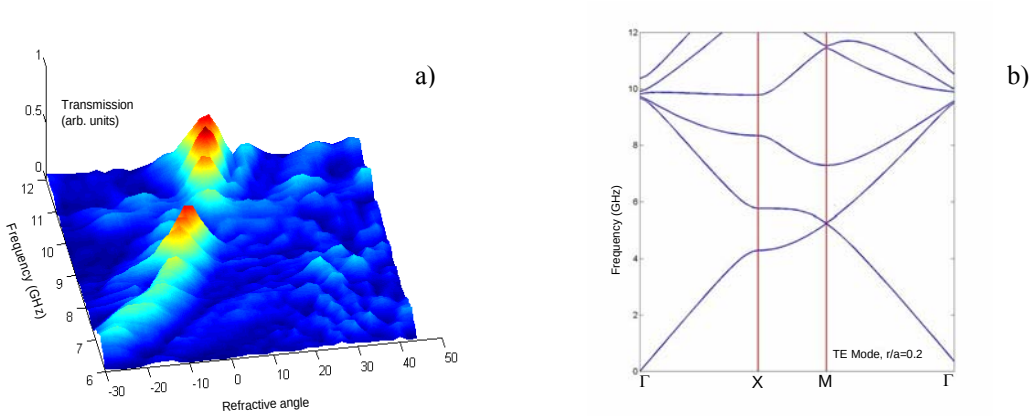

Fig. 3 3 a shows a 3D experimental plot of the magnitude of the field versus frequency and angle of refraction and Fig. 3 b shows the band structure calculation for triangular lattice PC with r/a=0.2 in TE mode

We have also carried out measurements of refraction for TE mode propagation. The band structure for TE mode is shown in the figure 3. Here negative refraction is observed between 6.4 – 9.8 GHz and positive refraction between 9.8 -12 GHz. It is important to note that negative refraction is possible for both TM and TE modes; such a freedom in the choice of modes provides a crucial advantage of using the metallic PC over the split ring wire array metamaterial.

3.1. Band Structure Calculations

The physical principle behind the present results can be understood from the band structure of the metallic PC. We have calculated the band structure of the triangular lattice PC employing a finite difference method. For the TM modes, the electric field can be identified with the wave function of a 2D periodic δ-shell potential barrier, thus a plane wave expansion method can be used to calculate the band structure. The 2D band structures of both TM and TE are shown respectively in Figs. 2 (b1) and 3(b). For a plane wave with incident wave vector $\vec{k}_i$ and frequency ω incident normally on an air-PC interface, the wave vector $\vec{k}_f$ inside the PC is parallel or anti-parallel to $\vec{k}_i$ as determined by the band structure. For a general case the phase velocity $\vec{v}_p = (c/|n_p|)\hat{k}_f$ with $\hat{k}_f = \vec{k}_f / |\vec{k}_f|$ and the group velocity $\vec{v}_g = \nabla_{\vec{k}}\omega$ can have any angle between them. Thus distinction must be made between negative wave vector refraction and negative group refraction.

An effective refractive index can be defined $n_p = \mathrm{sgn}(\vec{v}_g \vec{k}_f) c|\vec{k}_f| / \omega$ and calculated from the band structure. The sign of n_p is determined from the behavior of the EFS. Negative wave vector refraction will happen if $\vec{v}_g \cdot \vec{k}_f < 0$ while negative group refraction will be present only if $\vec{v}_g \cdot (\vec{k}_f - \vec{\kappa}) < 0$ with $\vec{\kappa}$ is the center of the equi-frequency surface (EFS) ellipsoid. Note that the direction of the group velocity $\vec{v}_g$ in an infinite PC coincides with that of the energy flow. If only the zero-th order Bragg wave refraction is present, conservation of the $\vec{k}_f$ component along the surface of refraction would result in positive or negative wave vector refraction, depending on whether $\vec{k}_f$ is parallel or anti-parallel to group velocity.

If higher order Bragg wave refraction is present, the emerging beam can be written as $\Psi_t = a_0 e^{i\vec{k}_{t0}\cdot\vec{r}} + a_1 e^{i\vec{k}_{t1}\cdot\vec{r}}$ where $\vec{k}_{t0}$ and $\vec{k}_{t1}$ represent the refracted wave vectors corresponding to the 0^{th} and 1^{st} order Bragg wave-vectors of the

field inside the PC. 2nd and higher order Bragg wave refraction is ignored. Let the component of $\vec{k}_t$ along the normal to the surface of refraction of the prism be $k_{t\perp}$. One has $k_{t0\perp} = \sqrt{\omega^2/c^2 - k_f^2 \sin^2\theta}$ and $k_{t1\perp} = \sqrt{\omega^2/c^2 - (2\pi/a - k_f \sin\theta)^2}$ where θ=π/3 is the incident angle at the second surface of the prism and a is the lattice periodicity. The parallel component is $k_{t\|} = k_f \sin\theta$. The refracted angle can be obtained from $\theta_r = \tan^{-1}(k_{t\|}/k_{t\perp})$ for each beam.

From the band structure and the EFS for TM mode of propagation negative refraction is predicted for the second and third band regions, with positive refraction in the 1st band. In the 1st band between 6-7.1GHz the EFS move outward with increasing frequency, so that $\vec{v}_g \cdot \vec{k}_f > 0$. In the second band between 8.3-11 GHz, the EFS move inward with increasing frequency, consistent with $n_p < 0$ corresponding to $\vec{v}_g \cdot \vec{k}_f < 0$ ($\vec{v}_g$ anti-parallel to $\vec{k}_f$). The band gap is in the frequency range 7.1-8.3 GHz between the 1st and 2nd pass-bands and from 11-11.2 GHz between the second and third bands.

3.2. Discussion

TM MODE

The agreement between experimental results of refraction and those deduced from band structure calculation is remarkable. In Fig 3(c) the representative experimental results show that negative and positive refraction are present in different frequency ranges.

I. In the first band between 6 – 7.1 GHz the refraction is positive, consistent with $n_p > 0$ from the band structure and corresponding to RHE $\vec{v}_g \cdot \vec{k}_f > 0$. The representative plot at f = 6.68 GHz, Fig. 2(a1) shows that the signal is largely in the positive direction.

II. In the second band between 8.3 – 11 GHz, the refraction is negative for the zero'th order Bragg wave refraction, consistent with $n_p < 0$ from the band structure and corresponding to LHE $\vec{v}_g \cdot \vec{k}_f < 0$. There is observed also a first order Bragg wave that is positively refracted in the same frequency window. This branching of the beams observed in metallic rods in air design can be eliminated in a dielectric PC design, where only a single beam can be observed. Two illustrative plots corresponding to 9.315 and 10.77 GHz show that the signal is strongly peaked in the negative direction and becomes stronger with the increase in frequency.

III. A band gap is clearly observed in the experiment, which matches with the band structure, in the region between 7.1-8.3 GHz. As can be seen from the 3D plot figure the transmission through the PC is near zero.

TE MODE

It is important to note that negative refraction is possible for TE mode as well. Such a freedom in the choice of modes is a crucial advantage of using the metallic PC over the split ring wire array metamaterial.

I. In the first band between 6.4 – 9.8 GHz the zero'th order Bragg wave refraction is negative, consistent with $n_p < 0$ and $\vec{v}_g \cdot \vec{k}_f < 0$ from the band structure and corresponding to LHE. The bandwidth of this negative band is 39% which is quite a remarkable improvement.

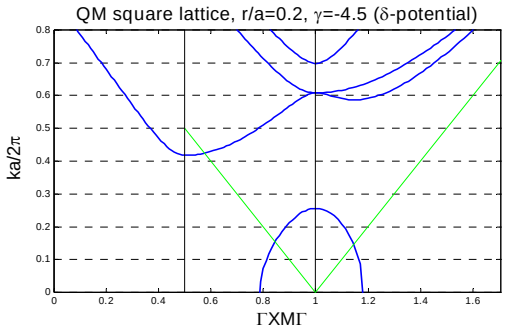

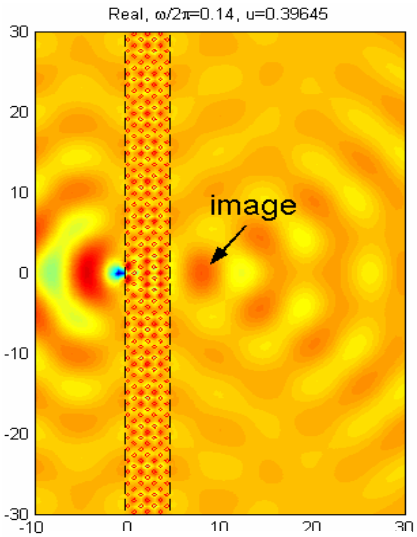

Flat lens image of a periodic delta-shell potential

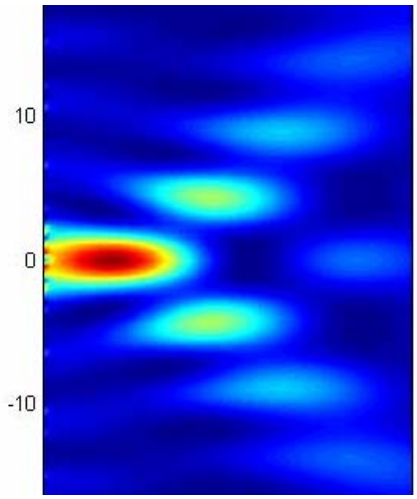

The intensity of the transmitted wave function.

Fig. 4 a) Band structure of a periodic delta-shell potential of a square lattice. The straight lines are light lines b) Flat lens image of a periodic delta-shell potential c) The intensity of the transmitted wave function.

II. In the second band between 9.8 – 12 GHz, the refraction is largely positive, consistent with $n_p > 0$ from the band structure and corresponding to RHE $\vec{v}_g \cdot \vec{k}_f > 0$.

III. The absence of a band gap from 6-12GHz along GM Brillion zone propagation direction as predicted by the band structure calculation is in complete agreement with experimental results shown in Fig 3a.

3.3. Imaging by a Flat Lens

Negative refraction using LHM leads to entirely new and fascinating concepts for image formation. One of the most striking consequences of NR is the ability of flat surfaces to focus a divergent beam and hence leads to imaging of an object placed near the lens. A negative index flat lens reconstructs not only the far field propagating waves, but can also reconstruct evanescent waves.

Image formation is wave reconstruction of both far and near fields. We have developed a new approach to imaging by a **flat** lens made of a proposed artificial metamaterial [xii]. The key aspect of a flat lens using LHM is the absence of an optical axis. In contrast, current flat lenses like the Fresnel lens, which use gradient-index refractive material (GRIN), and all have an optical axis. The conditions for image formation are determined by the requirement that the phase shift $\Phi = \int \vec{k} \cdot d\vec{l}$ from object to image is independent of wave vector for all directions. Flat lens imaging can be achieved by fabricating a material which has appropriate dispersion relations $\omega(\vec{k})$. The intrinsic parameters that define the new material are σ, which is determined by the dispersion characteristics of the material, and κ, which is a measure of the phase shift $\exp(i\sigma\kappa d)$ by the flat slab. This is a generalization of Pendry's flat lens with elliptic dispersion $k_x^2 + \sigma^{-2}(k_z - \kappa)^2 = \omega^2 / c^2$ and negative group refraction $\vec{v}_g \cdot (\vec{k}_f - \vec{\kappa}) < 0$. The lens equation for a slab of thickness *d* is determined to be $u+v=\sigma d$. Here *u* and *v* are the distances of the object and the image from the nearest surfaces. *Unlike GRIN, the effective refractive index is angle dependent* $n(\theta)$, *not spatial dependent* $n(x)$. The lens constant κ determines whether the lens has positive or negative refractive index n_p and gives rise to a phase shift of the image $\exp(i\sigma\kappa d)$. Simulations of image formation by such a material are shown in Fig.7. The space inside the slab appears to be stretched by a factor of σ. "Perfect" images are achieved when the material is suitably matched to its environment as shown in the figure. We have shown that this material can be realized approximately using photonic crystals to achieve the desired $\omega(\vec{k})$.This preliminary theoretical investigation of a special material for flat lens imaging is entirely novel and can lead to new designs for flat lenses. The theoretical principles that we have obtained will be used to design novel flat lenses made of metamaterials and photonic crystals. The main goal is to design a material with suitable characteristics leading to minimal reflection and "perfect" imaging.

In our flat lens experiment the image is imperfect and reveals the presence of satellites – this is due to the fact that the propagation is along the so-called $\Gamma \to X$ for a square lattice in the 2nd band where the inside the crystal the 1st Bragg wave-vector is involved. A better image should be achieved with propagation along the $\Gamma \to M$ in the first band where also the negative group refraction condition can be satisfied. Under this condition a single image should be possible. More generally the best conditions of imaging are achieved when the equifrequency surfaces are circular or nearly so, and consistent with negative refraction.

NUMERICAL SIMULATIONS OF FLAT LENS IMAGING

To understand flat lens imaging, we consider a model system which is a periodic δ-shell potential $V(r) = \gamma \sum_j \delta(|\vec{r} - \vec{R}_j| - r_0)$. For $\gamma \to \infty$, the wave function must vanish on the disk boundary. The wave function is equivalent to the electric field of the TM modes of a metallic PC. We have used this model to simulate negative refraction in metallic PC. For attractive potential $\gamma < 0$, and within appropriate energy window, negative refraction and flat lens imaging of waves can be achieved. Below is a band structure of a square lattice for γ=-4.5 and r_0/a=0.2 with lattice spacing *a*. It is predicted that above $ka/2\pi$=0.14, all-angle-negative-refraction can be achieved along the ΓM direction.

The flat lens imaging of a point source $-\frac{i}{4}H_0(kr)$ is shown below at $k\,a/2\pi = 0.14$ with a distance $u = 0.4a$ away from the first surface. A clear image is seen on the other side of the slab at v=4.70*a*. This gives an effective σ_{eff}=1.03 which is consistent with the EFS. When the source is moved away from the first surface of the slab, the image will move toward the second surface. When u > σd, virtual image will be seen through ray-tracing.

The mechanism of sub-wavelength imaging is due to the bounded states of the δ-shell potential. The surface waves are not present if no δ-shell is broken.

For real photonic crystals or the above δ-shell potential model, the effective refractive index σ is angle dependent. At certain frequency and with appropriate design, the EFS can be elliptic with negative group refraction, the image can

have high quality with small aberration. Otherwise, the image will be blurred due to aberration. Our flat lens theory can be used to design high quality flat lens.

4. Conclusion

The phenomenon of negative refraction in periodic media embodied by photonic crystals is well established by the experiments described above. The imaging and focusing experiments also show that entirely novel concepts are possible due to NR. Optical components utilizing NR are expected to have several advantages such as enabling sub-wavelength resolution, flat lenses without optical axis thus avoiding optical alignment, and improved performance such as due to reduced aberration for the same structural dimensions. In addition light weight and compact structures offer additional advantages in a variety of applications.

We thank Beverly Turchenetz and Richard Wing for invaluable contributions. This work was supported by the National Science Foundation and the Air Force Research Laboratories, Hanscom AFB (contract #F33615-01-1-1007).

[i] R. A. Shelby, D. R. Smith, and S. Schultz, Science **292**, 77 (2001).
[ii] C. G. Parazzoli, R. B. Greegor, K. Li, B. E. C. Koltenbach, and M. C. Tanielian, Phys. Rev. Lett. **90**, 107401 (2003).

[iii] A. A. Houck, J. B. Brock, and I. L. Chuang Phys. Rev. Lett. **90**, 137401 (2003).

[iv] M. Notomi, Phys. Rev. B **62**, 10696 (2002); Opt. Quant. Elect. 34, 133 (2002).
[v] C. Luo, S. Johnson, J. Joannopoulos, and J. Pendry, Phys. Rev. B **65**, 201104 (2002).

[vi] J. B. Pendry, Phys. Rev. Lett. **85**, 3966 (2000).
[vii] P. V. Parimi, W. T. Lu, P. Vodo, and S. Sridhar, Nature(London) **426**, 404 (2003).
[viii] P.Vodo, P.Parimi, W.T.Lu, S.Sridhar, App. Phys. Lett. **86**, 201108 (2005).

[ix] P. V. Parimi, W. T. Lu, P. Vodo, J. B. Sokoloff, and S. Sridhar, Phys. Rev. Lett. **92**, 127401 (2004). .

[x] E. Cubukcu, K. Aydin, E. Ozbay, S. Foteinopoulou, and C. M. Soukoulis, Nature (London) **423**, 604 (2003)

[xi] P.Vodo, P.Parimi, W.T.Lu, S.Sridhar, App. Phys. Lett. **85**, 1858 (2004).

[xii] W.T. Lu and S. Sridhar, "Flat lens without optical axis: Theory of imaging", arXiv: cond-mat/0501715 (2005).